Noise-Adaptive Nonlinear Diffusion Filtering of MR Images With Spatially Varying Noise Levels

Alexei A. Samsonov[1,2*] and Chris R. Johnson[1]

Anisotropic diffusion filtering is widely used for MR image enhancement. However, the anisotropic filter is nonoptimal for MR images with spatially varying noise levels, such as images reconstructed from sensitivity-encoded data and intensity inhomogeneity-corrected images. In this work, a new method for filtering MR images with spatially varying noise levels is presented. In the new method, a priori information regarding the image noise level spatial distribution is utilized for the local adjustment of the anisotropic diffusion filter. Our new method was validated and compared with the standard filter on simulated and real MRI data. The noise-adaptive method was demonstrated to outperform the standard anisotropic diffusion filter in both image error reduction and image signal-to-noise ratio (SNR) improvement. The method was also applied to inhomogeneity-corrected and sensitivity encoding (SENSE) images. The new filter was shown to improve segmentation of MR brain images with spatially varying noise levels. Magn Reson Med 52:798–806, 2004. © 2004 Wiley-Liss, Inc.

Key words: magnetic resonance imaging; inhomogeneity correction; sensitivity encoding (SENSE); anisotropic diffusion filtering

MR images often require postacquisition noise filtering before they are visually inspected or noise-sensitive postprocessing methods are applied (1). As a rule, such filtering is desired to significantly decrease image noise and, simultaneously, to preserve fine image details in the image. Anisotropic diffusion (2) is an accepted filtering technique that provides such image enhancement. The anisotropic diffusion filter is suitable for practical use because of its computational speed and algorithmical simplicity. The filter assumes that image noise is Gaussian-distributed, which is valid for SNR > 3 (3). The anisotropic diffusion filter has proved to be a valuable preprocessing tool for MR image segmentation (1,4,5), MRI inhomogeneity correction (6), and robust myelin water quantification (7).

Another issue concerning MR image noise that one should consider before applying noise filters is how the noise is spatially distributed. Noise has uniform spatial distribution for images reconstructed from Cartesian data. However, a number of reconstruction and postprocessing techniques create images with spatially nonuniform noise. Examples include images that are multiplicatively corrected for intensity inhomogeneity (6,8), and images obtained with partially parallel imaging (PPI) techniques (9–15). Nonuniformity of image noise is especially pronounced in the latter case. Decreased acquisition times and amplified noise errors lead to increased and spatially varying image noise levels. The problem becomes worse at high speedup factors. Special techniques, such as numerical conditioning (15), second-pass reconstruction (16), and phase-constrained image refinement (17), have been proposed in an effort to overcome noise amplification. These methods may significantly decrease noise amplification; however, they are not capable of improving image SNR behind the fundamental limits established by MRI theory (18). Retrospective denoising with a nonlinear technique, such as anisotropic diffusion filtering, is an appealing option for improving the SNR of PPI images.

This work addresses the problem of anisotropic diffusion filtering of MR images with spatially varying noise. It was previously demonstrated (5) that the anisotropic diffusion filter is efficient for refining MR images characterized by noise levels that are unvarying in the image plane. In this study we show that the standard anisotropic diffusion filter is nonoptimal for filtering the images with spatially nonuniform noise. Application of the filter can result in excessive blurring of image structures in low-noise areas and/or enhancement of noise-generated image gradients in high-noise regions. We propose to couple a filtering parameter of the anisotropic diffusion filter with local noise statistics to overcome the problem. The rest of the paper is organized as follows: First, we provide background on anisotropic diffusion filtering and its robust statistical formulation. Next, we describe a new noise-adaptive method and give implementation details. We then provide quantitative and qualitative results from the method validation and comparison with the standard filter. Last, we discuss the new method's advantages and limitations.

THEORY

Anisotropic Diffusion Filtering of MR Images With Spatially Uniform Noise Levels

Anisotropic diffusion filtering in the Perona-Malik formulation (2) can be achieved by solving the following partial differential equation with respect to the image function $I(\bar{r}, t)$:

$$\frac{\partial I(\bar{r}, t)}{\partial t} = \nabla(g(\|\nabla I\|, k) \cdot \nabla I(\bar{r}, t)), \quad [1]$$

where $g(\|\nabla I\|, k)$ is a monotonically decreasing diffusivity function, ∇I is an image gradient, k is a conductance

[1]Scientific Computing and Imaging Institute, University of Utah, Salt Lake City, Utah.

[2]Department of Physics, University of Utah, Salt Lake City, Utah.

Grant sponsor: NIH BISTI; Grant number: 1P20HL68566-01.

*Correspondence to: Alexei A. Samsonov, Scientific Computing and Imaging Institute, University of Utah, 50 S. Central Campus Drive, Room 3490, Salt Lake City, UT 84112. E-mail: samsonov@sci.utah.edu

Received 23 July 2003; revised 13 May 2004; accepted 13 May 2004.

DOI 10.1002/mrm.20207

Published online in Wiley InterScience (www.interscience.wiley.com).

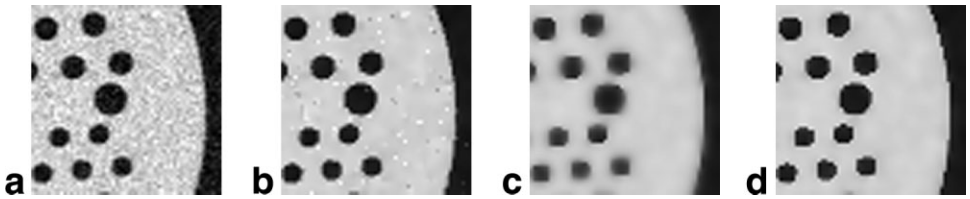

FIG. 1. Effect of parameter *k* on the performance of the standard anisotropic diffusion filter. **a:** Original image ($\sigma_{noise} = 0.0418$); **b–d:** Images filtered in 30 iterations using *k* equal to σ_{noise}, $4\sigma_{noise}$, and $2\sigma_{noise}$, respectively. The low value of *k* (**b**) leads to the enhancement of high-noise-generated gradients, which could be incorrectly identified as meaningful structures. Filtering with high *k* (**c**) results in significant blurring of edges. Filtering with optimal *k* (**d**) results in the preservation of edges and noticeable improvement of the SNR.

parameter, and *t* is an artificial time parameter. Parameter *k* defines a threshold between image gradients to be smoothed and image gradients to be preserved. With a proper choice of *k*, the filter provides efficient noise removal in homogeneous image regions, while preserving tissue boundaries and enhancing edge sharpness.

For analysis purposes, we use a robust statistical formulation of an anisotropic diffusion filter (19). The filtering problem is formulated as an estimation of a piecewise-constant image function from noisy data, using a robust error norm ρ:

$$\min_{I} \int_{\Omega} \rho(\|\nabla I\|, \sigma_e)\, d\Omega, \qquad [2]$$

where σ_e is a parameter bounding the values of the possible outliers. In MR images, these outliers correspond to image gradients generated by tissue boundaries. The formulation is equivalent to the Perona-Malik filter under a gradient descent minimization of Eq. [2], if the diffusivity function is chosen as

$$g(x, k) = \frac{1}{x} \frac{\partial \rho(x, \sigma_e)}{\partial x},$$

$$k = c\sigma_e, \qquad [3]$$

where *c* is a scaling coefficient.

Gerig et al. (5) demonstrated that the filter is highly efficient for magnitude-reconstructed MR images. They pointed out that *k* should be kept as small as possible to preserve the boundaries of anatomical structures of small contrast in MR images. Too small a value of *k,* however, would result in the preservation and enhancement of high-noise-related gradients (20). Figure 1 demonstrates the effect of optimal and suboptimal choices of *k* on the result of the anisotropic diffusion filtering.

The optimal anisotropic diffusion filter should diminish the enhancement of noise-related image gradients, and at the same time minimize smoothing of the anatomical structure boundaries. Apparently, *k* should be coupled with image noise properties. The parameter *k* is routinely chosen as a constant for traditional MR images with spatially uniform noise levels. Such a choice becomes nonoptimal for images with spatially varying noise, as demonstrated in the Results section.

Noise-Adaptive Diffusion Filtering of MR Images With Spatially Varying Noise Levels

Assume that the MR image can be modeled as a piecewise constant (slowly varying) function. This assumption is valid for MR images that have only low-frequency intensity inhomogeneity, such as that induced by body or head coils. In addition, assume that the image is corrupted by additive zero-mean Gaussian noise.

Let the noise values for each pair of adjacent pixels *m* and *n,* with intensities I_m and I_n, be uncorrelated and have predetermined variances of σ_m^2 and σ_n^2. Consider a difference $\Delta_{mn} = I_n - I_m$ to be minimized with the chosen robust error norm to accomplish the anisotropic diffusion filtering (Eq. [2]). If pixels *m* and *n* belong to the same tissue type, the distribution of the difference Δ_{mn} is zero-mean Gaussian (Fig. 2):

$$\Delta_{mn} \in N(0, \sigma_{mn}),\ \sigma_{mn} = \sqrt{\sigma_m^2 + \sigma_n^2}. \qquad [4]$$

Difference Δ_{mn}^e across an intensity discontinuity, such as a tissue boundary, may be considered an outlier in the distribution ($\Delta_{mn}^e \notin N(0, \sigma_{mn})$) because it is formed by values from various populations (Fig. 2). We chose the threshold value for rejection of such outliers in the robust error norm as the population standard deviation (SD) $\sigma_e = \sigma_{mn}$. Correspondingly, the local conductance parameter is found from Eqs. [3] and [4]:

$$k_{mn} = c \cdot \sqrt{\sigma_m^2 + \sigma_n^2}. \qquad [5]$$

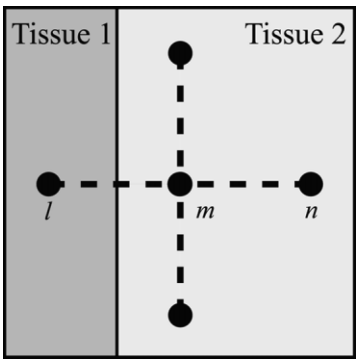

FIG. 2. Illustration of the robust statistical analysis of the anisotropic diffusion filter.

Parameter k is now dependent on the local noise properties. Image gradients that are unlikely to be generated by noise values and corresponding to tissue boundaries will be preserved, and the corresponding image structure will be enhanced. Also, the gradients bounded by local noise level will be smoothed. This improves the image SNR and simultaneously minimizes the enhancement of noise-related image gradients.

The scaling coefficient c in Eq. [5] can be found for each type of diffusivity function using the condition that the contribution of image gradients to the functional in Eq. [2] decreases at σ_e (19). This occurs when the derivative of the influence, or flow, function $\psi(x, k) = x \cdot g(x, k)$ is zero:

$$\left.\frac{\partial \psi(x,\ c\sigma_e)}{\partial x}\right|_{x=\sigma_e} = 0. \qquad [6]$$

For example, for the exponential diffusivity function (2)

$$g(\|\nabla I\|,\ k) = \exp(-(\|\nabla I\|/k)^2), \qquad [7]$$

c is $\sqrt{2}$. This yields

$$k_{mn} = \sqrt{2} \cdot \sqrt{\sigma_m^2 + \sigma_n^2}. \qquad [8]$$

This result agrees with the choice of the conductance parameter in Ref. 5 for filtering the MR images with spatially uniform noise levels. In that work, k for the exponential diffusion function was experimentally selected to be in the interval $[1.5\sigma_{noise},\ 2\sigma_{noise}]$, where σ_{noise} is the image noise SD. The choice agrees with Eq. [8]: if the noise level is spatially uniform, then $\sigma_n = \sigma_m = \sigma_{noise}$, and $k_{mn} = 2\sigma_{noise}$.

Algorithm: Noise-Adaptive Nonlinear Diffusion

for each pixel m
  Find $k_{mp} = \sqrt{2} \cdot \sqrt{\sigma_m^2 + \sigma_p^2}$,
$p \in \{l,n,i,j\}$ (Fig. 3)
end
$I^{(0)}$ = Noisy Image
for $t = 0 \ldots$(Number of Iterations-1)
  for each pixel m
    Calculate $G_{mp}^{(t)} = I_p^{(t)} - I_m^{(t)}$ and $D_{mp}^{(t)} = g(G_{mp}^{(t)}\ k_{mp})$
$p \in \{l,n,i,j\}$ (Fig. 3)
    Create new estimate of pixel m:
$$I_m^{(t+1)} = I_m^{(t)} + \Delta t \cdot \sum_{p \in \{l,n,i,j\}} G_{mp}^{(t)} \cdot D_{mp}^{(t)}$$
  end
end

The method was implemented in MATLAB 6.1 and run on a Pentium 4 1.7GHz PC with 1Gb of RAM. The algorithm requires a noise distribution map as an input to provide noise-adaptation. Obtaining noise maps is an application-dependent procedure. As an example, we outline methods for obtaining noise maps for SENSE and inhomogeneity-corrected images.

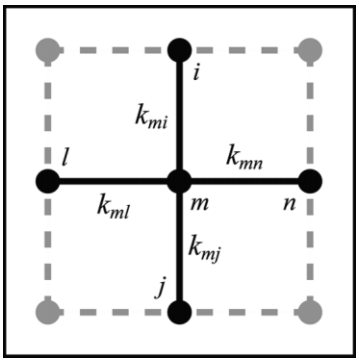

FIG. 3. Four-point discretization scheme for the diffusion equation approximation.

MATERIALS AND METHODS

Implementation Details

We chose to use an explicit final difference method (21) to discretize Eq. [1]:

$$I_m^{(t+1)} = I_m^{(t)} + \Delta t \cdot \sum_{p \in \eta(m)} \nabla I_{mp}^{(t)} \cdot g(\nabla I_{mp}^{(t)},\ k_{mp}), \qquad [9]$$

where $\eta(m)$ is the discretization neighborhood of pixel m, $\nabla I_{mp}^{(t)}$ is an finite difference approximation of the derivative of the image function, and Δt establishes the diffusion rate. The range of acceptable time steps Δt depends on the discretization scheme used (21).

A standard four-point neighborhood discretization scheme was utilized ($\Delta t \in (0,\ 0.25)$) (Fig. 3). The algorithm uses an original image as an initial guess, and proceeds with a fixed number of iterations as follows:

SENSE Image Noise

The properties of noise in SENSE images reconstructed from Cartesian data (Cartesian SENSE) are described by an image noise matrix given by (9):

$$\mathbf{X} = \frac{1}{n_k}(\mathbf{S}^{\mathbf{H}}\boldsymbol{\Psi}^{-1}\mathbf{S})^{-1}, \qquad [10]$$

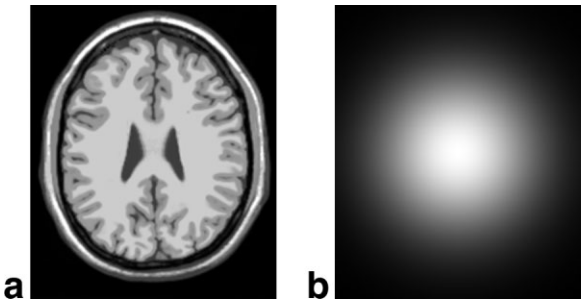

FIG. 4. Simulation study data. **a:** Digital brain phantom **b:** Noise map.

where **S** is the sensitivity matrix, n_k is the number of sampling positions in *k*-space, * denotes the Hermitian conjugate operation, and $\mathbf{\Psi}$ is the receiver noise matrix. Matrix $\mathbf{\Psi}$ describes noise levels and correlations in the acquisition channels for the given imaging setup, and is used for SNR-optimized reconstruction. The diagonal of **X** represents noise variances in the unfolded pixels, while the off-diagonal elements give the noise correlations among them. In Cartesian SENSE, the noise correlation due to reconstruction occurs only among values of distant pixels obtained on each unfolding step. This long-range correlation can be safely neglected, as the developed filter usually involves only short-scale diffusion smoothing.

The estimation of noise levels in a SENSE image starts with the construction of a relative noise map N_R from the diagonal entries of matrix **X.** To reflect true noise statistics, the map should be scaled with an image-dependent proportionality constant:

$$N_T = \chi N_R. \quad [11]$$

If the receiver noise matrix $\mathbf{\Psi}$ used in Eq. [10] is factual for the collected data, then $\chi = 1$, and the noise map N_R contains the absolute image noise variances. If $\mathbf{\Psi}$ is obtained in a scan with different acquisition parameters, or is taken as the identity for simplicity, χ must be determined in a separate procedure. Our approach for finding χ is to analyze the samples from air background areas of the reconstructed image. The method proceeds as follows:

1) Let $\mathbf{\Omega}$ be a part of the air background area in the reconstructed image that contains only noise contributions. To avoid including correlated noise values in the estimation, choose $\mathbf{\Omega}$ so that its linear size, in the direction of aliasing, is limited by the size of the decreased FOV. If coil sensitivity is not defined in $\mathbf{\Omega}$, an arbitrary function can be chosen so that the sensitivity matrix is not singular (different linear trends for each coil may be used).

2) Reconstruct the pixels $I_{\mathbf{\Omega}}$ belonging to $\mathbf{\Omega}$, find the noise map $N_{R,\mathbf{\Omega}}$ in the area, and normalize $I_{\mathbf{\Omega}}$ as

$$I_{\mathbf{\Omega}}^{norm} = I_{\mathbf{\Omega}} / \sqrt{N_{R,\mathbf{\Omega}}}. \quad [12]$$

3) Find the SD σ_n of $|I_{\mathbf{\Omega}}^{norm}|$, and use it to obtain the normalization constant:

$$\chi = \sigma_n^2/(2 - \pi/2). \quad [13]$$

Here the denominator accounts for a change in the variance of pixels in the air background due to the magnitude reconstruction (22).

Noise in Inhomogeneity-Corrected Images

Intensity inhomogeneity correction is often applied to MR images before other postprocessing techniques, such as thresholding-based image segmentation, are used. The goal of this correction is to retrospectively compensate for a number of imaging effects that lead to a discrepancy in intensity of the same tissue type in different image parts. The correction involves a priori and/or retrospective estimation of the gain field $G(\boldsymbol{r})$, which is used for multiplicative image intensity correction. The procedure creates images with spatially varying noise levels. The spatial distribution of noise variances in the corrected images is given by:

$$N_R = G^2(\boldsymbol{r}). \quad [14]$$

Again, the noise distribution should be scaled (Eq. [13]) to reflect the overall noise level.

Data

For validation, we used a realistic digital phantom of the human brain that is available on the Internet (http://www.bic.mni.mcgill.ca/brainweb) (T_1 weighting, image size = 181 × 217; Fig. 4a). Phantom construction was based on a low-noise data set that was segmented and preprocessed to create the anatomical brain model. The available datasets were created by calculating the NMR signal from a simulation of pulse sequences based on the Bloch equations (23,24). Zero-mean Gaussian noise (SD = 0.1 of white matter intensity) was modulated by a Gaussian function (max = 1 in the image center; Fig. 4b), and then added to real and imaginary image channels. Filter performance was evaluated in terms of root-mean-squared (RMS) error and an SNR improvement factor. The SNR improvement factor is defined as a ratio of pixel noise SDs before and after application of the filter. We used the following test to evaluate improvement of the SNR because image-based evaluations of noise parameters are not robust, due to the unknown behavior of the noise level in filtered images. First, we produced 100 instances of the digital phantom image with different realizations of noise contamination. Then we estimated SNR improvement factors for image pixels belonging to white matter, gray matter, and cerebrospinal fluid (CSF) areas by analyzing the pixel values from the multiple images.

Additionally, the methods were tested on real MRI data. Informed consent was obtained from all volunteers in accordance with our institution's policies regarding human subjects. Data were acquired on a 1.5T GE SIGNA MR scanner (GE Medical Systems, Milwaukee, WI) using a custom-built, four-element ($N_c = 4$), bilateral phased-array coil (25). Phantom data were obtained with a standard fast spin-echo (FSE) sequence (ETL = 16, BW = 32 kHz, TE = 20 ms, TR = 1000 ms, image matrix = 256 × 256). Brain data were obtained with a dual-contrast FSE pulse se-

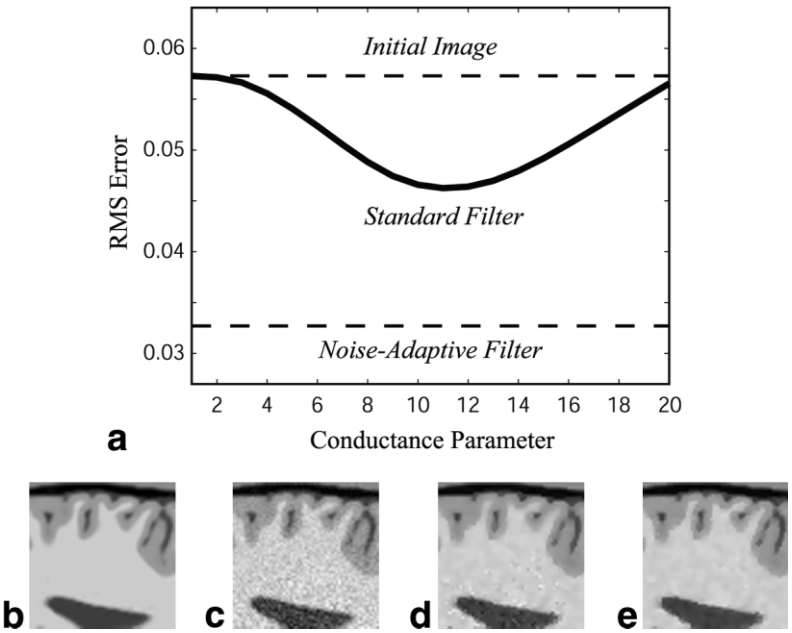

FIG. 5. Results of simulation studies (single image, 15 iterations). **a:** RMS error of standard filter vs. conductance parameter (the range of the parameter corresponds to the range for noise-adaptive filter). Levels of RMS error for initial and noise-adaptive filtered images are shown by dashed lines. **b-e:** ROI of reference image, noisy image, and images filtered with "best RMS." Conductance parameter and noise-adaptive anisotropic diffusion, respectivley.

quence (ETL = 16, BW = 20.83 kHz, TE = 33/99 ms, TR = 3000 ms, image matrix = 256 × 256).

Coil sensitivity profiles were used for inhomogeneity correction and SENSE image reconstruction. We obtained profiles from reference data using a local polynomial fit procedure described in Ref. 9, and separated the air background by thresholding the reference data. In the SENSE experiments, background pixels were excluded from reconstruction. The receiver noise matrix Ψ was chosen as the identity in all experiments, and the scaling factor χ was obtained by an analysis of air background pixels.

Both standard and noise-adaptive anisotropic diffusion filters were implemented with an exponential diffusivity function (Eq. [7]) and a time discretization step $\Delta t = 0.25$.

RESULTS

Simulation Studies

Figure 5 shows the results of filtering a single digital phantom image. The standard filter was applied with several values of the conductance parameter uniformly distributed in the range required for the noise-adaptive filter. The plot of RMS error vs. conductance parameter (Fig. 5a) suggests that, although the standard filter is less optimal for RMS error reduction than the proposed noise-adaptive filter, there is a value of the conductance parameter that minimizes the image error. This value was estimated from the plot and used to produce the image shown in Fig. 5d. Clearly, noise values are not completely filtered in all areas. The figure demonstrates one type of filtering error caused by a nonoptimal choice of the conductance parameter. The residual noise has a spike-like appearance, and could easily be mistaken for small anatomical features that are not present in the reference image (Fig. 5b).

The results of studying the SNR improvement factor on a series of noisy digital phantom images are shown in Fig. 6. As can be appreciated from the plots, a standard filter provided higher SNR for a tiny fraction of pixels, but the overall improvement of SNR is behind the noise-adaptive filter. The improvement provided by our new filter is further confirmed by measurements summarized in Table 1. The noise-adaptive filter leads to a much lower RMS error. The SNR improvement factor for the noise-adaptive filter

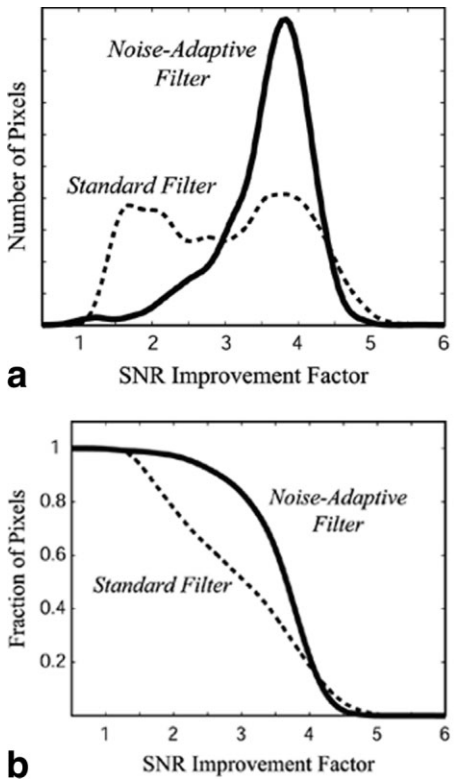

FIG. 6. Results of simulation studies (100 instances of noisy digital phantom image, 15 iterations of filters). **a:** Histogram of SNR improvement factor. **b:** Plot showing a fraction of pixels for which SNR was improved at least by a factor given on horizontal axis.

Table 1
Performances of Standard and Noise-Adaptive Filters*

	Standard filter	Noise-adaptive filter
Mean of SNR improvement factor	3.02	3.57
STD of SNR improvement factor	0.99	0.63
Mean of RMS error	0.047	0.033
STD of RMS error	3.70e-4	3.56e-4

*The study was conducted on 100 noisy digital brain phantom images (15 iterations, mean of RMS of noisy images was 0.058).

is characterized by a higher mean and a smaller SD than the standard filter. Therefore, in addition to the decreased image error, the noise-adaptive filter produces a more uniform SNR improvement in the image plane than the standard filter. The time per iteration was about 0.1 s both for standard and for noise-adaptive filters.

Phantom Experiments

Figure 7 shows the results of filtering the inhomogeneity-corrected phantom image. We removed the inhomogeneity using a priori estimated coil sensitivities, as described in Ref. 26. For the standard anisotropic diffusion filter, we considered two limiting choices of k: the first was optimal for filtering high-noise areas ("high-noise" filtering), and the second was optimal for filtering the low-noise areas ("low-noise" filtering). Values of k were chosen with the use of corresponding maximum and minimum noise variances in the noise map. In the absence of a ground truth, we used the absolute value of the difference between the original and filtered images to evaluate filter performance. For "high-noise" anisotropic diffusion, our results revealed substantial blurring of the boundaries of the phantom structures (Fig. 7e). Another type of error caused by the nonoptimality of standard filtering is degradation of resolution. With the "low-noise" k, the anisotropic diffusion filter leaves unfiltered noise in the image (Fig. 7d). The difference for an image filtered with noise adaptation shows that edges are not significantly degraded in the filtered image (Fig. 7c). At the same time, noise is efficiently removed in areas with both low and high noise levels (Fig. 7h). Filtering the image with a conductance parameter taken as a mean value of the image noise map enhances high-noise-generated image gradients, leading to spike artifacts (Fig. 7g) similar to those described in the Simulation Studies section.

In Vivo Experiments

Figure 8 shows the results of filtering SENSE images reconstructed from patient brain data. Nonoptimal coil positioning and limited coil sensitivity depth gave rise to a noise map with significant (up to 5 times) nonuniformity and large discontinuity (Fig. 8b). In the absence of a ground truth, the difference between the original and filtered images demonstrated filter performance in each case. The results indicate that "low-noise" k led to the enhancement of noise-generated gradients in high-noise areas that could be incorrectly identified as anatomical structures of different tissue types characteristic for the imaging modality (for example, vessels and CSF (Fig. 8e)). The "high-noise" k led to unnecessary oversmoothing of the image structures, such as vessels and brain tissue boundaries, in all areas (Fig. 8g). The difference (Fig. 8h) contains a number of correlated structures with intensity well above local noise levels, indicating a loss of resolution. In contrast, the noise-adaptive filter provided good retention of the image structures, and decreased image noise (Fig. 8c and d).

Figure 9 presents the results obtained when we studied the effect of noise-adaptive filtering on MR brain image segmentation. We reconstructed the image from fully encoded proton-density-weighted multicoil MRI data using known sensitivities profiles. The image contains an inhomogeneity component induced by the body coil sensitivity that should be corrected for robust thresholding-based image segmentation. The inhomogeneity map was modeled as a second-order Legendre polynomial whose parameters were estimated by means of an information minimization approach (8). Histograms of the images on different post-processing stages are shown in Fig. 9b. As can be appreciated from the plots, the inhomogeneity correction improves mode separation in the image histogram, which is further improved when applied with the new method. The intensity segmentation threshold was taken as a point of local minimum between two main modes of the corresponding histogram. The results of segmenting the noisy and filtered images using the threshold value are presented in Fig. 9c and d, respectively. We eliminated outer scalp tissues using a mask created by flood-filling the largest connected component in the initial binary image. The segmentation results indicate that noise in the initial image led to the misclassification of many image pixels, especially in the central image area where noise levels were high (Fig. 9c). The application of the noise-adaptive filter improved classification of such pixels (Fig. 9d). As a result, the segmented areas now have improved integrity.

DISCUSSION

An ideal filter for MR images with spatially varying noise levels must be able to improve the image SNR while preserving important image structures and avoiding the generation of artifacts. Nonlinear filters based on an anisotropic diffusion process are often the methods of choice to satisfy these criteria. However, images filtered with widely used standard anisotropic diffusion filter, with parameter k chosen as a constant in all image areas, may suffer from increased image errors. Errors arise from excessive smoothing in high-SNR areas, leading to a loss of spatial resolution (Figs. 7e and 8h), and from unfiltered noise in low-SNR regions, resulting in the generation of small image structures with a spike-like appearance (Figs. 5d and 7g). Obviously, the errors become more pronounced for images with strongly nonuniform noise levels, such as PPI and inhomogeneity-corrected images.

The noise-adaptive anisotropic diffusion filter developed in this research is characterized by an optimized behavior that allows filtering errors to be minimized (Fig. 5, Table 1). The efficiency of our method comes from its noise-adaptive nature, which is provided by a priori knowledge of the spatial dependency of the image noise. The new method also produces a more uniform SNR im-

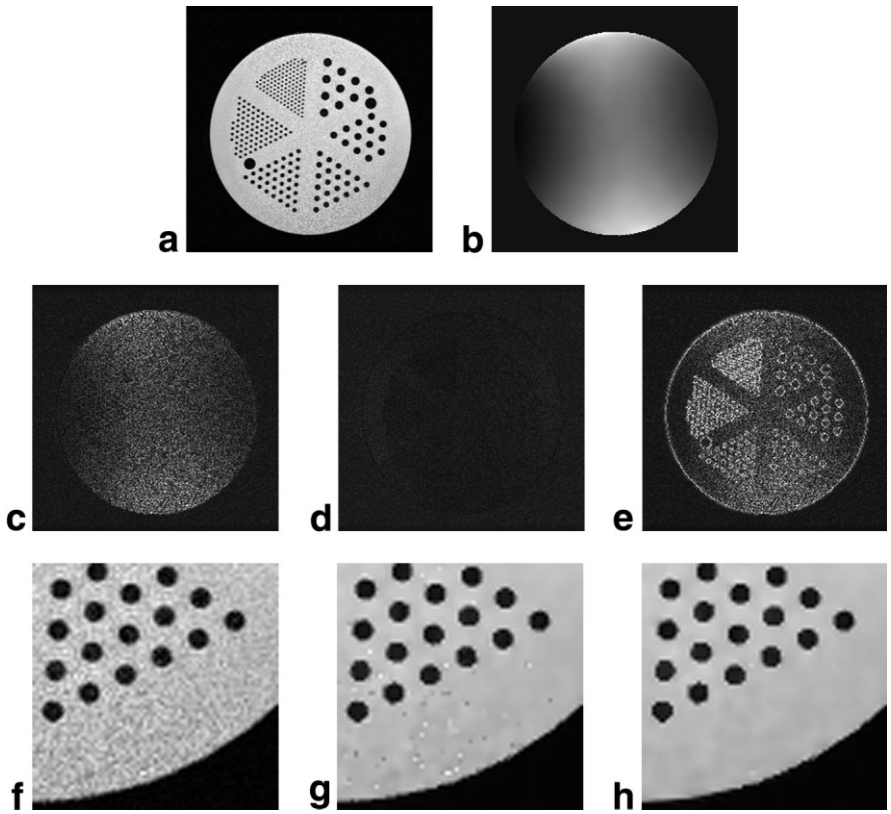

FIG. 7. Application of filters to inhomogeneity-corrected phantom image (25 iterations). **a:** Initial image. **b:** Map of noise SD. **c–e:** Absolute values of the differences between the original image and images filtered with the noise-adaptive filter and low- and high-noise *k* standard filters, respectively. **f–h:** ROI of initial image, image filtered with mean value of *k*, and noise-adaptive anisotropic diffusion filters, respectively.

provement in the image plane compared to that obtained with the standard method (Fig. 6). The image enhancement provided by the new filter is beneficial for intensity-based image segmentation of brain images with spatially varying noise. The new method can be used with the majority of existing MR image processing techniques that use anisotropic diffusion filtering as the initial stage (4,6,7).

The new noise-adaptive anisotropic diffusion filter is an attractive option for increasing the SNR of PPI images. Such images are characterized by a reduced SNR, which often limits the application of PPI techniques. We used SENSE images to test our noise-adaptive filter. A similar approach can be taken for other PPI techniques that provide information on spatial noise distribution (27). Noise adaptation for SENSE data does not incur significant computational overhead, since the calculation of the partial image noise matrix (Eq. [10]) is a part of the reconstruction procedure (9). The application of the proposed method to SENSE images reconstructed from arbitrary trajectories is challenging due to the nonavailability of the image noise matrix in feasible iterative approaches (28). One solution is a simulation-based noise map determination. Another application of the new filter might be to produce the image estimate needed for feedback reconstruction techniques (16,17).

The determination of the image noise level from background area samples is not always robust, because of artifacts (motion-related ghosting, etc) or limited size of the areas. In such cases, alternative approaches for estimating the noise level should be used. Gerig et al. (5) reported successful noise parameter retrieval from homogeneous areas detected with a special procedure. An attractive approach is to estimate image noise by collecting a sufficient number of signal-free samples (with radiofrequency pulses turned off) along with data acquisition.

This new method could possibly be extended to the filtering of image derivatives (29), which could be beneficial for images that strongly deviate from the piecewise constant (slowly varying) model (i.e., images obtained from surface coil images by a sum-of-squares approach). The principles outlined in this work could be easily extended to other techniques based on the nonlinear diffusion process (30,31). Generalization of the method to the 3D case and the filtering of multicontrast data is straightforward.

CONCLUSIONS

We have developed a new method for denoising images with spatially varying noise that can arise in MRI. This new method can improve image SNR and minimize image errors that may arise from the application of the standard anisotropic diffusion filter. The standard anisotropic diffusion filter, with a constant conductance parameter, proved to be nonoptimal in the presence of noise with spatially varying level.

The efficiency of the new method was demonstrated on simulated data and on SENSE and inhomogeneity-corrected images. The image enhancement provided by the new technique proved beneficial for improving the quality of segmentation of MR images with spatially varying noise. The automatic choice of parameters, and the overall effi-

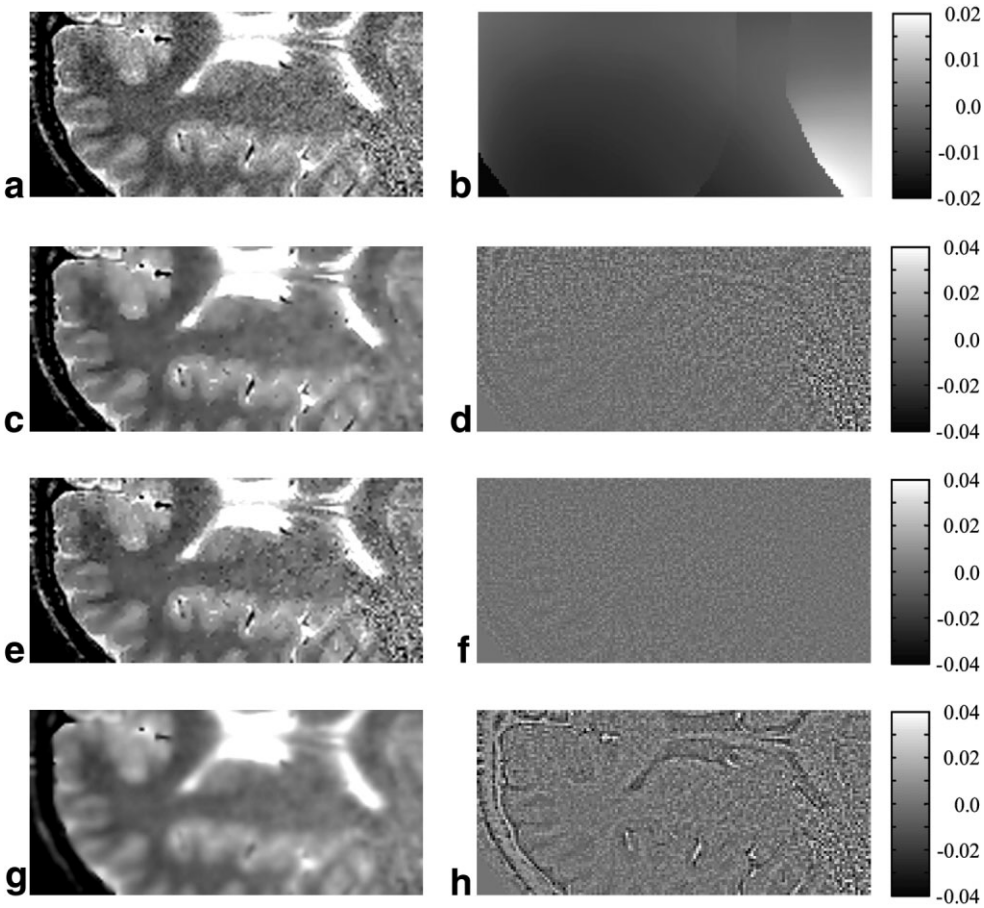

FIG. 8. Anisotropic diffusion filtering of a brain image (T_2 weighting, SENSE, $N_c = 3$, $R = 2$, 10 iterations). **a:** Initial image. **b:** Corresponding noise map. **c**, **e**, and **g:** Results of filtering initial image with noise-adaptive filter, low-noise anisotropic diffusion, and high-noise anisotropic diffusion, respectively. **d**, **f**, and **h:** Difference between image **a** and images **c**, **e**, and **g**, respectively.

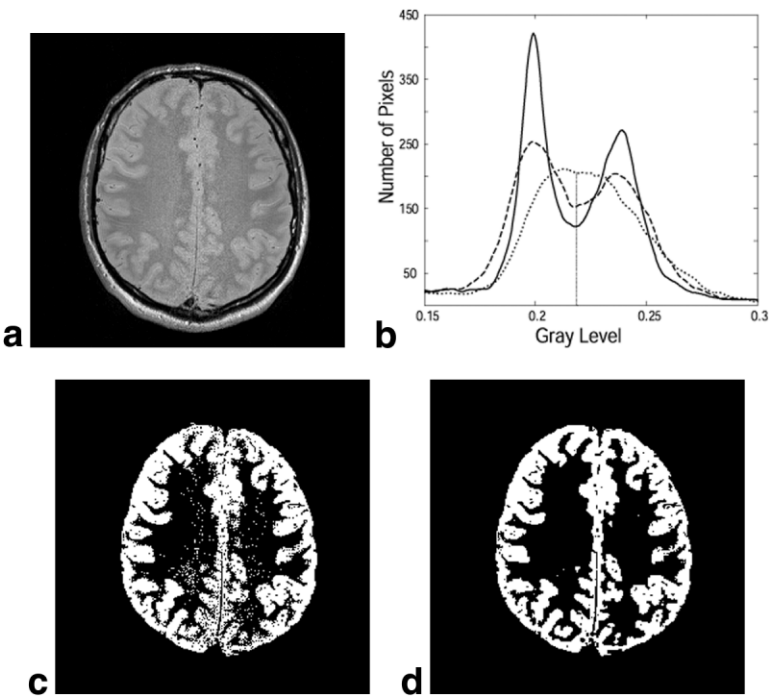

FIG. 9. Effect of noise-adaptive anisotropic filtering on MR image segmentation. **a:** Initial image. **b:** Histograms of initial (dotted), inhomogeneity-corrected (dashed), and filtered (solid) images. The segmentation threshold is indicated by the dash-dotted vertical line. **c** and **d:** Segmented areas of nonfiltered and noise-adaptive filtered images, respectively.

ciency of the method make it suitable for improving the diagnostic quality of PPI images in clinical environments.

ACKNOWLEDGMENTS

The assistance of Dr. Eugene Kholmovski with the imaging experiments, and the valuable comments of Dr. Ross Whitaker are greatly appreciated.

REFERENCES

1. Clarke LP, Velthuizen RP, Camacho MA, Heine JJ, Vaidyanathan M, Hall LO, Thatcher RW, Silbiger ML. MRI segmentation: methods and applications. Magn Reson Imaging 1995;13:343–368.
2. Perona P, Malik J. Scale-space and edge detection using anisotropic diffusion. IEEE Trans Patt Anal Machine Intell 1990;12:629–639.
3. Gudbjartsson H, Patz S. The Rician distribution of noisy MRI data. Magn Reson Med 1995;34:910–914.
4. Atkins MS, Mackiewich B. Fully automatic segmentation of the brain in MRI. IEEE Trans Med Imaging 1998;17:98–107.
5. Gerig G, Kubler O, Kikinis R, Jolesz FA. Nonlinear anisotropic filtering of MRI data. IEEE Trans Med Imaging 1992;11:221–232.
6. Styner M, Brechbuhler C, Szckely G, Gerig G. Parametric estimate of intensity inhomogeneities applied to MRI. IEEE Trans Med Imaging 2000;19:153–165.
7. Jones CK, Whittall KP, MacKay AL. Robust myelin water quantification: averaging vs. spatial filtering. Magn Reson Med 2003; 50:206–209.
8. Likar B, Viergever MA, Pernus F. Retrospective correction of MR intensity inhomogeneity by information minimization. IEEE Trans Med Imaging 2001;20:1398–1410.
9. Pruessmann KP, Weiger M, Scheidegger MB, Boesiger P. SENSE: sensitivity encoding for fast MRI. Magn Reson Med 1999;42:952–962.
10. Sodickson DK, Manning WJ. Simultaneous acquisition of spatial harmonics (SMASH): ultra-fast imaging with radiofrequency coil arrays. Magn Reson Med 1997;38:591–603.
11. Bydder M, Larkman DJ, Hajnal JV. Generalized SMASH imaging. Magn Reson Med 2002;47:160–170.
12. Griswold MA, Jakob PM, Heidemann RM, Haase A. Parallel imaging with localized sensitivities (PILS). Magn Reson Med 2000;44:243–251.
13. Kyriakos WE, Panych LP, Kacher DF, Westin CF, Bao SM, Mulkern RV, Jolesz FA. Sensitivity profiles from an array of coils for encoding and reconstruction in parallel (SPACE RIP). Magn Reson Med 2000;44:301–308.
14. Griswold MA, Jakob PM, Heidemann RM, Nittka M, Jellus V, Wang J, Kiefer B, Haase A. Generalized autocalibrating partially parallel acquisition (GRAPPA). Magn Reson Med 2002;47:1202–1210.
15. Sodickson DK, McKenzie CA. A generalized approach to parallel magnetic resonance imaging. Med Phys 2001;28:1629–1643.
16. Tsao J, Pruessmann KP, Peter Boesiger P. Feedback regularization for SENSE reconstruction. In: Proceedings of the 10th Annual Meeting of ISMRM, Honolulu, 2002. p 739.
17. Samsonov AA, Kholmovski EG. Method for quality improvement of images reconstructed from sensitivity-encoded data. In: Proceedings of the 10th Annual Meeting of ISMRM, Honolulu, 2002. p 2408.
18. Parker DL, Gullberg GT. Signal-to-noise efficiency in magnetic resonance imaging. Med Phys 1990:17:250-257.
19. Black MJ, Sapiro G, Marimont DH, Heeger D. Robust anisotropic diffusion. IEEE Trans Image Processing 1998:7:421-432.
20. Weickert J. Anisotropic diffusion in image processing. Stuttgart: Teubner-Verlag; 1998. 170 p.
21. Golub GH, Ortega JM. Scientific computing: an introduction with parallel computing. Boston: Academic Press; 1993. 442 p.
22. Edelstein WA, Bottomley PA, Pfeifer LM. A signal-to-noise calibration procedure for NMR imaging systems. Med Phys 1984;11:180-185.
23. Collins DL, Zijdenbos A, Kollokian V, Sled JG, Kabani NJ, Holmes CJ, Evans AC. Design and construction of a realistic digital brain phantom. IEEE Trans Med Imaging 1998;17:463-468.
24. Kwan RKS, Evans AC, Pike GB. MRI simulation-based evaluation of image-processing and classification methods. IEEE Trans Med Imaging 1999;18:1085-1097.
25. Hadley JR, Chapman BE, Roberts JA, Chapman DC, Goodrich KC, Buswell HR, Alexander AL, Tsuruda JS, Parker DL. A three-coil comparison for MR angiography. J Magn Reson Imaging 2000;11:458-468.
26. Romer PB, Edelstein WA, Hayes CE, Souza SP, Mueller OM. The NMR phased array. Magn Reson Med 1990;16:192-225.
27. Sodickson DK, Griswold MA, Jakob PM, Edelman RR, Manning WJ. Signal-to-noise ratio and signal-to-noise efficiency in SMASH imaging. Magn Reson Med 1999;41:1009-1022.
28. Pruessmann KP, Weiger M, Scheidegger MB, Boesiger P. Advances in sensitivity encoding with arbitrary *k*-space trajectories. Magn Reson Med 2001;46:638–651.
29. Mrázek P. Nonlinear diffusion for image filtering and monotonicity enhancement. Ph.D. dissertation, Czech Technical University, Prague, 2001.
30. Parker GJM, Schnabelt JA. Enhancement of anisotropic diffusive filtering of MR images using approximate entropy. In: Proceedings of the 7th Annual Meeting of ISMRM, Philadelphia, 1999. p 175.
31. Keeling SL. Total variation based convex filters for medical imaging. Appl Math Comput 2003;139:101–119.